Journal of Solid State Chemistry **165,** 317–323 (2002)
doi:10.1006/jssc.2002.9538, available online at http://www.idealibrary.com on IDEAL®

Crystal Structures and Magnetic Properties of 6H-Perovskites $Ba_3MRu_2O_9$ (M = Y, In, La, Sm, Eu, and Lu)

Yoshihiro Doi,[1] Kazuyuki Matsuhira,[2] and Yukio Hinatsu

Division of Chemistry, Graduate School of Science, Hokkaido University Sapporo 060-0810, Japan

Received October 19, 2001; in revised form January 28, 2002; accepted February 8, 2002

Magnetic properties of quaternary oxides $Ba_3MRu_2O_9$ (M = Y, In, La, Sm, Eu, and Lu) are reported. Rietveld analyses of the X-ray diffraction data indicate that they adopt the 6H-perovskite structure and have the valence state of $Ba_3M^{3+}Ru_2^{4.5+}O_9$. All compounds are nonmetallic at least over the temperature range of 100–400 K. The magnetic susceptibilities show a broad maximum at 135–370 K except for the La compound, which shows a plateau around 22 K. In addition, another magnetic anomaly is observed at 4.5–12.5 K by the magnetic susceptibility and specific heat measurements for any compound. It is considered that this magnetic behavior is ascribed to the antiferromagnetic coupling between two Ru ions in a Ru_2O_9 dimer and to the magnetic interaction between the Ru_2O_9 dimers.

INTRODUCTION

Perovskites and perovskite-like oxides containing ruthenium often exhibit interesting magnetic and electrical properties. For example, strontium ruthenates $Sr_{n+1}Ru_nO_{3n+1}$ show interesting behavior. Sr_2RuO_4 is a superconductor below 0.93 K (1, 2) and $SrRuO_3$ is a metallic ferromagnet (T_c = 160 K) (3). Before now, we have studied the magnetic properties of ordered perovskites A_2LnRuO_6 (A = Sr, Ba; Ln = lanthanides), and have found very unique and complex magnetic behavior at low temperatures (4–8).

Recently, we have turned our attention to the magnetic properties of ruthenium-based oxides with the 6H-$BaTiO_3$ structure (9), which have the general formula $Ba_3MRu_2O_9$ (M = 3d transition metal, lanthanide elements, etc.). In many cases, these compounds have a hexagonal unit cell, and two kinds of the B site ions, Ru and M, occupy the face-sharing octahedral sites (Ru_2O_9 dimer) and the corner-sharing octahedral ones (MO_6 octahedron), respectively. This structure has a short Ru–Ru distance (2.48–2.69 Å), therefore, the strong magnetic interaction in the dimer is expected. Previously, Darriet *et al.* reported that the magnetic susceptibilities of $Ba_3M^{2+}Ru_2^{5+}O_9$ (M = Mg, Ca, Cd, and Sr) showed a broad maximum at 400–500 K and approached zero with decreasing temperature (10). These features were explained by the antiferromagnetic coupling of Ru^{5+} ions in the isolated dimer, which has the exchange integral $J = \sim -170$ K and the ground state of total spin $\mathbf{S} = \mathbf{S}_1 + \mathbf{S}_2 = 0$. Rath and Müller-Buschbaum measured the magnetic susceptibility of $Ba_3Y^{3+}Ru_2^{4.5+}O_9$ between 77 and 650 K (11). Its magnetic susceptibility showed a maximum at 220 K and did not obey the Curie–Weiss law.

When the $Ru_2^{4.5+}O_9$ dimer adopts a charge configuration of $Ru^{4+}Ru^{5+}O_9$, the total spin of a dimer may be $\mathbf{S} = \frac{1}{2}$ at sufficiently low temperatures. In that case, it is expected that not only the intra-dimer magnetic interaction but also the interaction between the dimers contribute to the magnetic properties of $Ba_3M^{3+}Ru_2^{4.5+}O_9$. However, there are few researches on this system, and their magnetic properties at low temperatures are not well known.

In this study, we prepared $Ba_3MRu_2O_9$ (M = trivalent ions, i.e., Y, In, La, Sm, Eu, and Lu), which are known to adopt the 6H-perovskite structures (12), and performed their X-ray diffraction measurements. In order to elucidate the magnetic behavior of $Ru_2^{4.5+}O_9$ dimer in the compounds, we have measured their magnetic susceptibility, specific heat, and electrical resistivity.

EXPERIMENTAL

Polycrystalline samples of $Ba_3MRu_2O_9$ (M = Y, In, La, Sm, Eu and Lu) were prepared by the conventional solid-state reaction. As starting materials, $BaCO_3$, RuO_2 and M_2O_3 were used. Before use, La_2O_3 and In_2O_3 were dried in air for a day at 900 and 800°C, respectively. They were weighed in an appropriate metal ratio and were mixed well in an agate mortar. The mixtures were pressed into pellets and then calcined at 900°C for 12 h. The calcined materials

[1] To whom correspondence should be addressed. Fax: +81-11-746-2557. E-mail: doi@sci.hokudai.ac.jp.

[2] Present address: Faculty of Engineering, Kyushu Institute of Technology, Kitakyushu 804-8550, Japan.

0022-4596/02 $35.00

were fired in air at 1100°C (for M = In) and 1200°C (for other samples) for 60–108 h with several interval grindings and pelletings. The heating-up ratio was 100°C/h. The progress of the reactions was monitored by powder X-ray diffraction measurements (XRD).

The XRD measurements were carried out at room temperature in the range $10^\circ \leq 2\theta \leq 120^\circ$ using a 2θ step size of 0.02° with Cu$K\alpha$ radiation on a Rigaku MultiFlex diffractometer. The data were analyzed by the Rietveld technique, using the program RIETAN2000 (13).

The temperature dependence of the magnetic susceptibilities was measured under both zero-field-cooled (ZFC) and field-cooled conditions (FC) in an applied field of 0.1 T over the temperature range 1.8–400 K using a SQUID magnetometer (Quantum Design, MPMS-5S).

Specific heat measurements were performed using a relaxation technique with a commercial heat capacity measurements system (Quantum Design, PPMS model) in the temperature range 1.8–300 K. The sintered sample in the form of a pellet was mounted on a thin alumina plate with grease for better thermal contact.

The temperature dependence of the resistivity was measured in the temperature range 100–400 K (for both cooling and heating process) using a DC four-probe technique with the same measurement system (PPMS model). The sintered samples were cut into pieces having sizes of approximately $5.0 \times 2.5 \times 1.2\ \text{mm}^3$. Four contact wires were painted onto the samples using silver paste.

RESULTS AND DISCUSSION

Crystal Structures

The results of the XRD measurements show that a series of $Ba_3MRu_2O_9$ (M = Y, In, La, Sm, Eu, and Lu) is formed in a single phase. The XRD patterns for La and Lu compounds are shown in Fig. 1. The data have been analyzed by the Rietveld method. It is confirmed that these compounds have the 6H-perovskite structure with space group $P6_3/mmc$

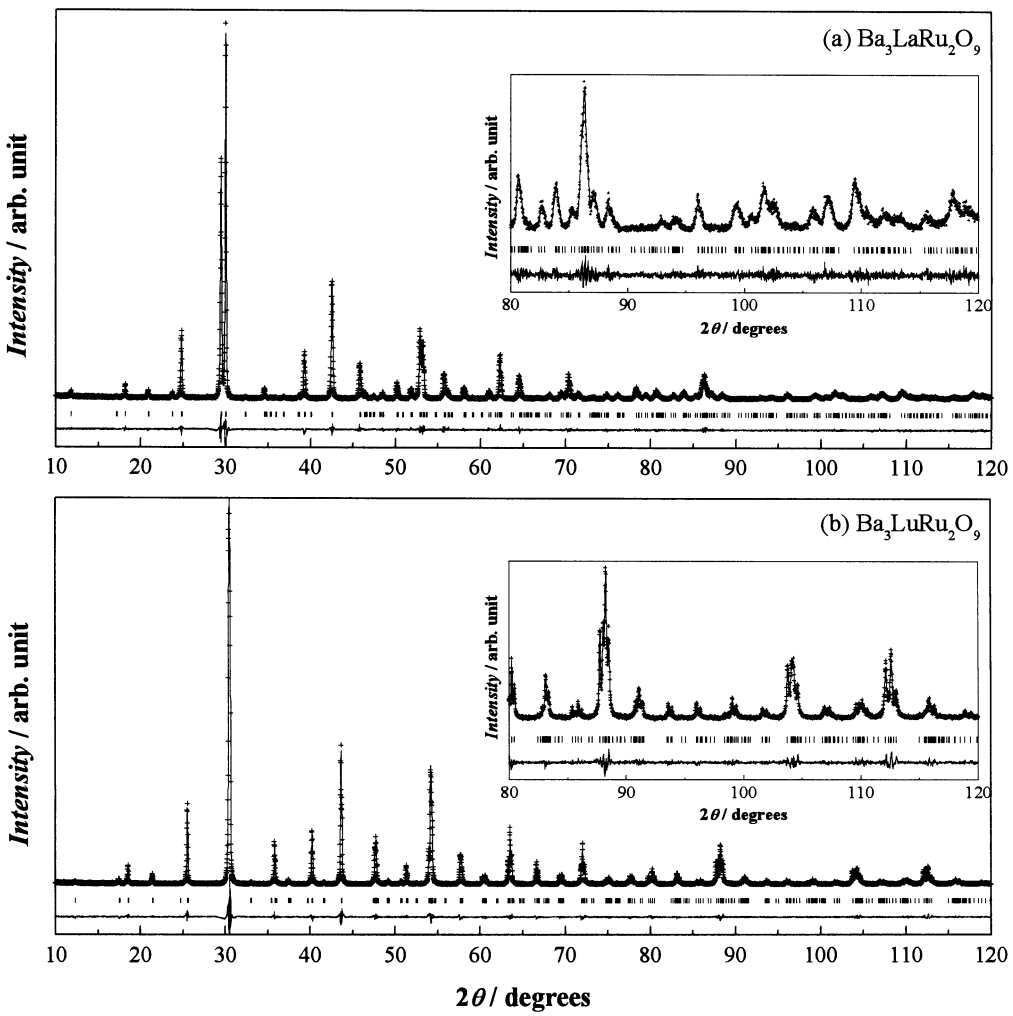

FIG. 1. X-ray diffraction profiles for (a) $Ba_3LaRu_2O_9$ and (b) $Ba_3LuRu_2O_9$.

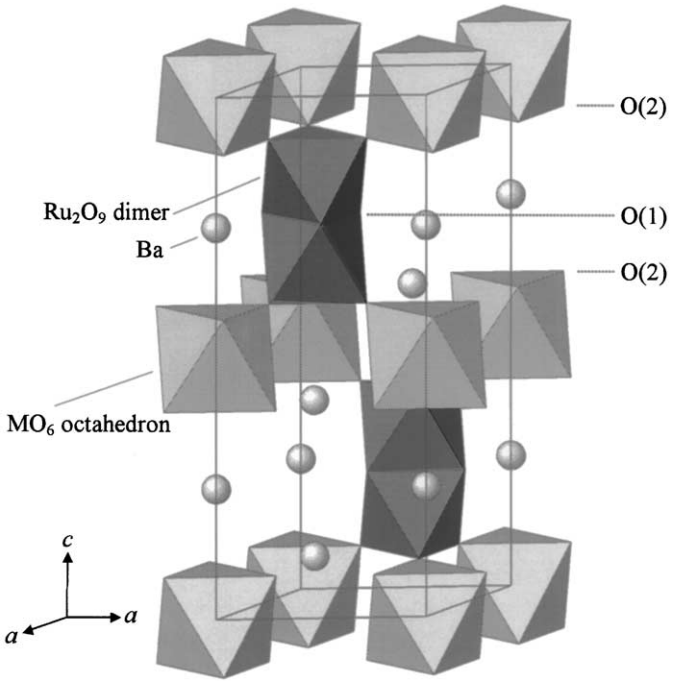

FIG. 2. The crystal structure of $Ba_3MRu_2O_9$.

(No. 194). The crystal structure of $Ba_3MRu_2O_9$ is schematically illustrated in Fig. 2. The cation sites within the face-sharing octahedra of this structure are occupied by ruthenium ions and those within the corner-sharing octahedra are occupied by M ions. The evidence that the cation disorder or oxygen defect occur has not been found. The structural parameters are summarized in Table 1.

Some selected bond lengths and angles are listed in Table 2. The lattice parameters and the M–O bond lengths increase monotonously with the size of the M^{3+} ion. Figure 3 shows the variation of the Ru–O(1), Ru–O(2) and the average Ru–O bond lengths with the ionic radius of M^{3+} ion. The results of previous studies for $Ba_3M^{3+}Ru_2^{4.5+}O_9$ (11, 14–17) are also plotted in this figure. The Ru–O(1) length increases with increasing ionic radius of M^{3+}, while the Ru–O(2) length decreases, therefore, the difference between them increases (see Fig. 3). This tendency clearly indicates that the shape of Ru_2O_9 dimers in the $Ba_3MRu_2O_9$ compounds is more distorted with increasing ionic radius of M^{3+}. The average Ru–O bond lengths are 1.976–1.985 Å. This value is in the middle between 1.989 and 1.997 Å for the $Ru_2^{4+}O_9$ dimer of $Ba_3LnRu_2O_9$ (Ln = Ce, Pr, and Tb) (18) and 1.965 Å for the $Ru_2^{5+}O_9$ dimer of $Ba_3MRu_2O_9$ (M = Zn and Ni) (19). This result indicates that the average valency of Ru ions is +4.5. The interatomic distances between two ruthenium ions (Ru–Ru) in the Ru_2O_9 dimer are 2.536–2.563 Å, which are longer than that in the $Ru_2^{4+}O_9$ dimer [2.481–2.493 Å (17, 18)] and shorter than that in the $Ru_2^{5+}O_9$ dimer [2.681–2.685 Å (11, 14, 17)]. These relations are also consistent with the above result.

TABLE 1
Structural Parameters for $Ba_3MRu_2O_9$

	M					
	Y	In	La	Sm	Eu	Lu
a(Å)	5.8816(2)	5.8185(3)	5.9579(3)	5.9192(3)	5.9133(3)	5.8542(2)
c(Å)	14.5010(4)	14.3145(7)	15.0058(8)	14.6788(7)	14.6346(6)	14.4163(4)
Ba(1) B(Å^2)	0.32(4)	0.48(9)	0.15(5)	0.70(8)	0.95(8)	0.40(5)
Ba(2) z	0.9061(1)	0.9101(1)	0.8947(1)	0.9029(1)	0.9041(1)	0.9077(1)
Ba(2) B(Å^2)	0.74(3)	0.47(4)	0.52(4)	0.70(5)	1.01(4)	0.61(3)
M B(Å^2)	0.05(6)	0.07(8)	0.1	0.10(8)	0.10(7)	0.08(4)
Ru z	0.1624(1)	0.1605(1)	0.1649(1)	0.1636(1)	0.1634(1)	0.1616(1)
Ru B(Å^2)	0.08(3)	0.04(5)	0.1	0.09(5)	0.10(4)	0.10(3)
O(1) x	0.4885(7)	0.4865(9)	0.4882(9)	0.4884(11)	0.4882(9)	0.4878(9)
O(1) B(Å^2)	0.7(2)	0.1(3)	0.3(3)	1.0(4)	1.0(3)	1.0(3)
O(2) x	0.1763(6)	0.1704(10)	0.1794(7)	0.1777(9)	0.1773(8)	0.1746(6)
O(2) z	0.4125(3)	0.4148(6)	0.4055(4)	0.4090(6)	0.4101(5)	0.4135(4)
O(2) B(Å^2)	0.8(1)	0.9(2)	1.1(2)	1.0(2)	1.0(2)	1.0(2)
R_{wp} (%)	11.86	15.94	13.06	15.69	13.73	13.32
R_I (%)	1.89	2.82	2.43	3.85	3.32	1.91
R_F (%)	1.08	2.03	1.77	2.28	2.02	1.40
R_e (%)	9.24	12.38	11.31	10.38	9.71	9.58

Note. Space group $P6_3/mmc$; $z = 2$. The atomic positions: Ba(1) $2b(0, 0, \frac{1}{4})$; Ba(2) $4f(\frac{1}{3}, \frac{2}{3}, z)$; M $2a(0, 0, 0)$; Ru $4f(\frac{1}{3}, \frac{2}{3}, z)$; O(1) $6h(x, 2x, \frac{1}{4})$; O(2) $12k(x, 2x, z)$. Definitions of reliability factors R_{wp}, R_I, R_F and R_e are given as follows:

$$R_{wp} = [\sum w(|F_o| - |F_c|)^2 / \sum w|F_o|^2]^{1/2}, \quad R_1 = \sum |I_{ko} - I_{kc}| / \sum I_{ko},$$

$$R_F = \sum |I_{ko}^{1/2} - I_{kc}^{1/2}| / \sum I_{ko}^{1/2}, \quad R_e = \left[(N - p) / \sum_i w_i y_i^2 \right]^{1/2}.$$

Electrical Resistivity

The resistivity of $Ba_3MRu_2O_9$ (M = Y, La, Sm, Eu, and Lu) is plotted as a function of reciprocal temperature in Fig. 4a. They are nonmetallic at least in the range

TABLE 2
Selected Bond Lengths (Å) and Angles (°) for $Ba_3MRu_2O_9$

	M					
	Y	In	La	Sm	Eu	Lu
Ba(1)–O(1)	2.943(1)	2.912(1)	2.981(1)	2.959(1)	2.962(1)	2.930(1)
Ba(1)–O(2)	2.963(6)	2.918(9)	2.979(7)	2.964(8)	2.960(9)	2.948(6)
Ba(2)–O(1)	2.901(4)	2.924(6)	2.847(6)	2.903(6)	2.894(7)	2.908(6)
Ba(2)–O(2)	2.944(1)	2.910(1)	2.986(1)	2.960(1)	2.963(1)	2.929(1)
Ba(2)–O(2)	3.078(5)	2.997(9)	3.393(6)	3.154(8)	3.190(9)	3.039(6)
Ru–O(1)	2.028(5)	2.006(7)	2.046(7)	2.030(7)	2.034(9)	2.019(7)
Ru–O(2)	1.934(5)	1.964(9)	1.908(7)	1.926(8)	1.918(9)	1.940(6)
Ru–O (average)	1.981(5)	1.985(8)	1.977(7)	1.978(7)	1.976(9)	1.980(6)
Ru–Ru	2.540(2)	2.563(4)	2.554(3)	2.536(3)	2.537(4)	2.549(3)
M–O(2)	2.199(5)	2.107(9)	2.332(7)	2.243(8)	2.260(9)	2.166(6)
Ru–O(2)–M	179.0(3)	177.9(5)	176.2(4)	178.0(4)	177.5(5)	178.8(3)
Ru–O(1)–Ru	77.5(3)	79.4(4)	77.2(3)	77.3(3)	77.2(4)	78.3(3)

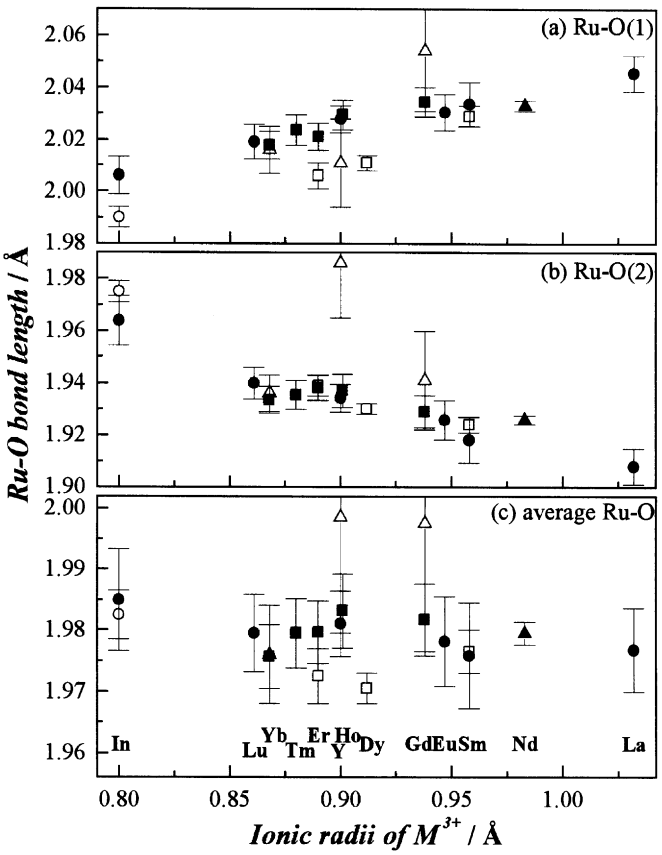

FIG. 3. Variation of the Ru–O bond lengths of $Ba_3MRu_2O_9$: (a) Ru–O(1), (b) Ru–O(2), and (c) average Ru–O lengths. *Note.* ●: present work, ▲: Doi *et al.* (14), ■: Doi *et al.* (15), ○: Rijssenbeek *et al.* (16), △: Rath *et al.* (11), and □: Müller-Buschbaum *et al.* (17).

$100 < T < 400$ K, showing increasing resistance with decreasing temperature. Attempts to fit the observed data to a simple Arrhenius model were unsuccessful. Then, the Mott variable-range hopping (VRH) model (20),

$$\rho \propto \exp((T_0/T)^{v}), \qquad [1]$$

was taken into account. In the case that the parameter v is $\frac{1}{3}$, i.e., the variable range hopping in two dimensions, experimental data show a good linearity (Fig. 4b). This result corresponds to the previous study for $Ba_3MRu_2O_9$ (M = Fe, Co, Ni, Cu, and In) (21) and $Ba_3LnRu_2O_9$ (Ln = Ce, Pr, and Tb) (18). The crystal structure of $Ba_3MRu_2O_9$ (Fig. 2) can be expressed by the alternate stacking of two kinds of two-dimensional layers which consist of the MO_6 octahedra or Ru_2O_9 polyhedra. This structural feature may account for the observed resistivity behavior.

Magnetic Susceptibility and Specific Heat

The temperature dependence of the magnetic susceptibilities (χ_M) for $Ba_3MRu_2O_9$ is plotted in Fig. 5. Except for the La compound, they show a broad maximum at 290 K (for M = Y), 370 K (In), 180 K (Sm), 135 K (Eu), and 345 K (Lu). The magnetic susceptibility of $Ba_3LaRu_2O_9$ shows a plateau at around 22 K. None of these compounds obey the Curie–Weiss law. In addition, it is found that they show another magnetic anomaly at low temperatures: 4.5 K (for M = Y), 4.5 K (In), 6.0 K (La), 12.5 K (Sm), 9.5 K (Eu), and 9.5 K (Lu).

The observed broad maxima above 100 K are similar to that found in the magnetic susceptibility vs temperature curves for $Ba_3M^{2+}Ru_2^{5+}O_9$ (M = Mg, Ca, Sr, and Cd) reported by Darriet *et al.* (10). They explained this behavior using a dimer model, in which two spins of Ru^{5+} ions in the Ru_2O_9 dimer couple antiferromagnetically. The effective magnetic moments per molecule are calculated from the equation $\mu_{eff} = 2.828\ (\chi_M\ T)^{1/2}$, and their temperature dependence is illustrated in Fig. 6a. They decrease gradually with decreasing temperature down to 0.24–0.45 μ_B at 1.8 K. Therefore, the magnetic interaction between Ru ions in the dimer is antiferromagnetic rather than ferromagnetic.

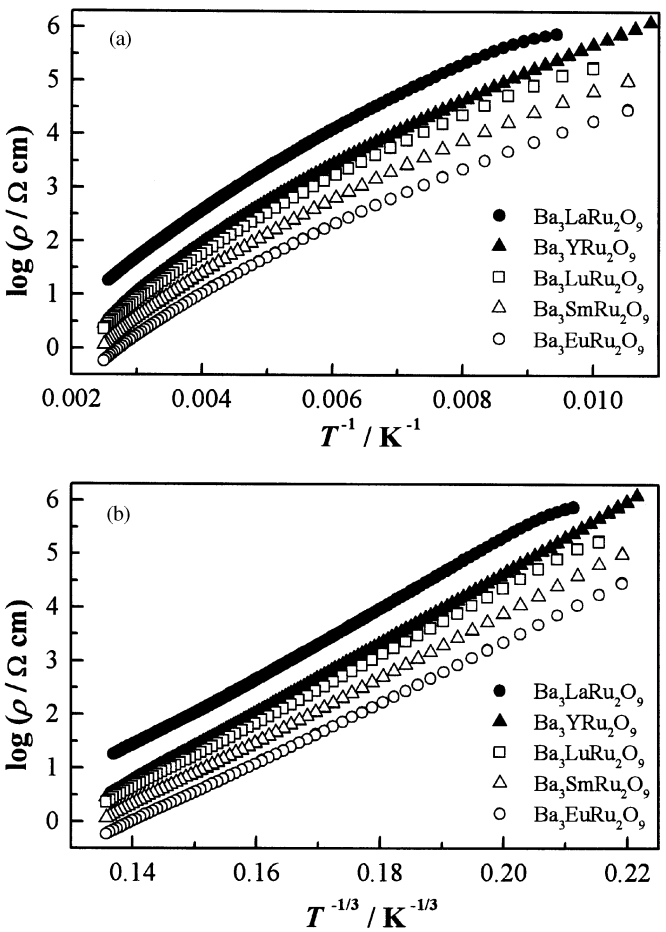

FIG. 4. Temperature dependence of the resistivity for $Ba_3MRu_2O_9$. (a) $\log \rho$ vs T^{-1} plot; (b) $\log \rho$ vs $T^{-1/3}$ plot.

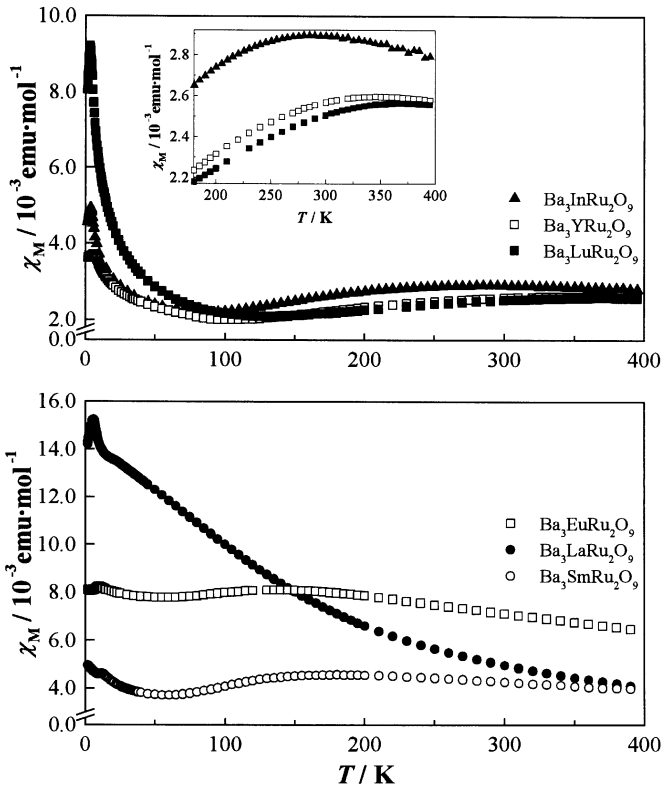

FIG. 5. Temperature dependence of the magnetic susceptibility for $Ba_3MRu_2O_9$: (a) M = Y, In, and Lu, (b) M = La, Eu, and Sm.

The spin Hamiltonian for the magnetic interactions of Ru ions in the Ru_2O_9 dimers is written as

$$H = -2J\mathbf{S}_1\cdot\mathbf{S}_2, \qquad [2]$$

where $\mathbf{S}_1$ and $\mathbf{S}_2$ are the spin operators and J is the exchange integral. Since the average valency of ruthenium ions is $+4.5$ in the title compounds, we applied the following dimer model to the observed magnetic susceptibilities; in this model, it is assumed that all dimers adopt a valence state of $Ru^{4+}Ru^{5+}O_9$ (i.e., d^4–d^3 dimer):

$$\chi_{45\mathrm{low}} = \frac{N_A g^2\mu_B^2}{3k_BT}\frac{3}{4}\frac{x^8+10x^5+35}{x^8+2x^5+3} \qquad [3]$$

or

$$\chi_{45\mathrm{high}} = \frac{N_A g^2\mu_B^2}{3k_BT}\frac{3}{4}\frac{x^{15}+10x^{12}+35x^7+84}{x^{15}+2x^{12}+3x^7+4}, \qquad [4]$$

where $x = e^{-J/k_BT}$, and N_A, g, μ_B, and k_B are Avogadro number, g factor, Bohr magneton and Boltzmann constant, respectively. Equations [3] and [4] express the magnetic susceptibility for the low-spin ($S_{Ru^{4+}} = 1$) dimers and that for the high-spin ($S_{Ru^{4+}} = 2$) dimers, respectively. The temperature dependence of the effective magnetic moments calculated from Eqs. [3] and [4] (for $g = 2$; $J = 50$, 200, -50, -100, -150, and -200 K) are plotted in Fig. 6b. The curves calculated for the positive J values do not match the experimental data. In the case of the negative J values, the temperature dependence of the calculated effective magnetic moments resembles the experimental data in the higher temperature region. They approach 1.732 μ_B (i.e., $S = \frac{1}{2}$ per dimer) with decreasing temperature; however, the experimental data are still smaller than this value. This result indicates that there exist the antiferromagnetic orderings of Ru_2O_9 dimers in these $Ba_3MRu_2O_9$ compounds. Measurements of the magnetic susceptibility and specific heat (as will be described later) show the anomalies at low temperatures due to these antiferromagnetic interactions.

Figure 7 shows the variation of the specific heat divided by temperature (C_p/T) as a function of temperature. An anomaly has been observed for each compound, which corresponds to the anomaly found at low temperatures in the magnetic susceptibility. For $Ba_3LaRu_2O_9$, a small specific heat anomaly has been found at 22 K, which is

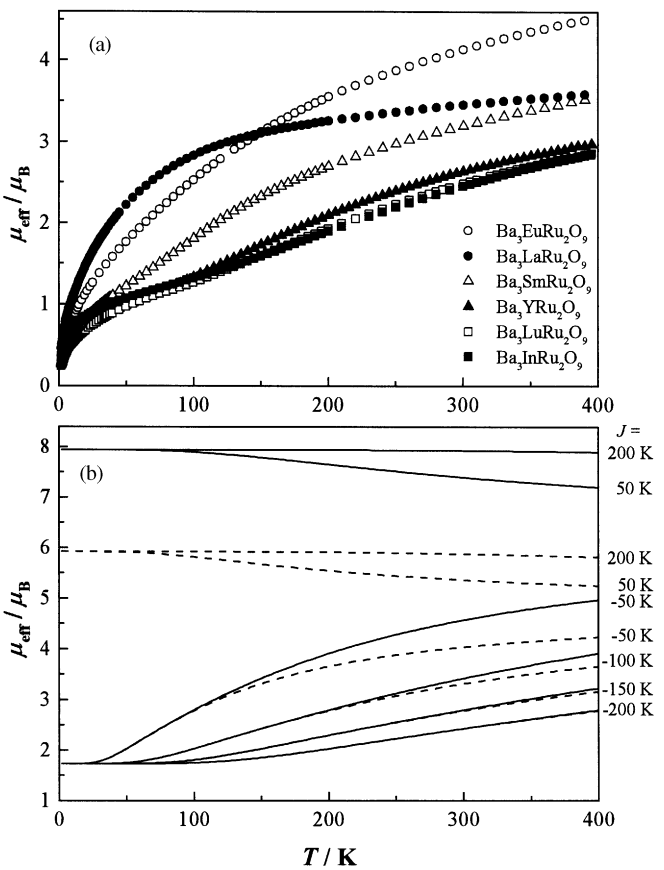

FIG. 6. Temperature dependence of the effective magnetic moment of $Ba_3MRu_2O_9$. The dashed and solid lines are the effective magnetic moments calculated by Eqs. [3] and [4], respectively.

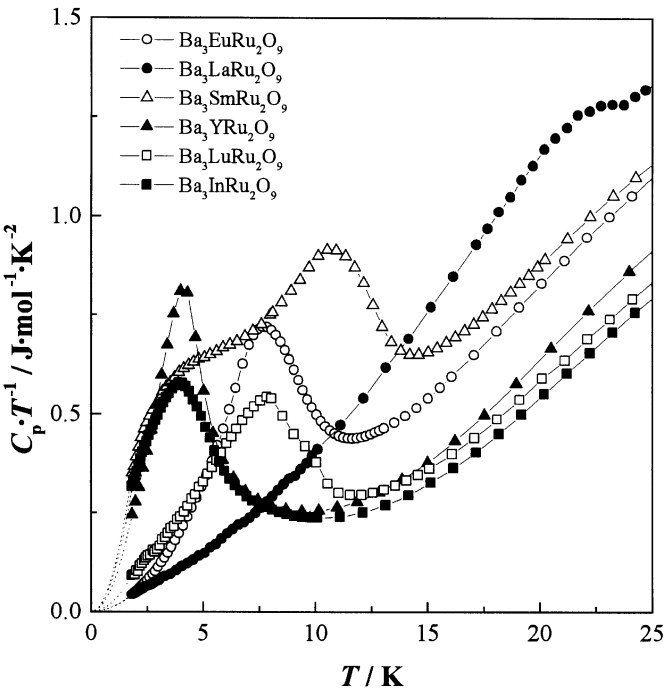

FIG. 7. Temperature dependence of the specific heat divided by temperature (C_p/T) for $Ba_3MRu_2O_9$. The dotted lines at low temperatures are the extrapolated curves of $C_p/T \propto T^2$.

consistent with the slight plateau observed in the susceptibility vs temperature curve at the same temperature. For $Ba_3SmRu_2O_9$, another broad anomaly has been observed at around 4 K.

The total entropy is calculated by $S_{\text{total}} = \int (C_p/T)\, dT$. In order to estimate the entropy below 1.8 K, the extrapolated curve of $C_p/T \propto T^2$ was used (see the dotted curves in Fig. 7). The temperature dependence of the total entropy is shown in Fig. 8. The entropy change derived from this magnetic anomaly is estimated to be approximately 3.0 J mol^{-1} K^{-1} (for M = Y, In, Eu, Lu), 6.0 J mol^{-1} K^{-1} (for M = Sm), and 0.3 J mol^{-1} K^{-1} (for M = La). These magnetic entropy changes correspond to the antiferromagnetic orderings of Ru_2O_9 dimers. The value of 3.0 J mol^{-1} K^{-1} is smaller than the expected value $R \ln(2S+1) = R \ln 2 =$ 5.76 J mol^{-1} K^{-1}. This may be due to the occurrence of the short-range magnetic ordering at higher temperatures than the respective magnetic transition temperatures. The entropy change for $Ba_3SmRu_2O_9$ is larger than those for the others. It contains two entropy changes for the anomalies at 12.5 and 4 K observed in the C_p/T vs temperature curve. The anomaly at 12.5 K is due to the antiferromagnetic ordering between Ru_2O_9 dimers and that at 4 K is possibly a Schottky-type one which is caused by the energy level splitting of the ground doublet Γ_7 of Sm^{3+} ions in the internal magnetic field. For $Ba_3EuRu_2O_9$, the entropy change is very close to that of $Ba_3MRu_2O_9$ (M = nonmagnetic Y^{3+}, In^{3+}, and Lu^{3+} ions). This fact indicates that the Eu^{3+} is a nonmagnetic ion with the $J = 0$ ground state.

The temperature dependence of the magnetic susceptibility and specific heat for $Ba_3LaRu_2O_9$ is different from that for the other $Ba_3MRu_2O_9$, i.e., its magnetic susceptibility has a slight plateau at around 22 K without showing any maximum, and the entropy change for the magnetic anomaly estimated from the specific heat measurements is much smaller than those for the other $Ba_3MRu_2O_9$ compounds. These differences in the magnetic behavior may arise from the RuO_6 polyhedron in the Ru_2O_9 dimer distorted greatly from the regular octahedron.

CONCLUSIONS

The 6H-perovskites $Ba_3MRu_2O_9$ (M = Y, In, La, Sm, Eu, and Lu) have a valence state of $Ba_3M^{3+}Ru_2^{4.5+}O_9$. The shape of Ru_2O_9 dimers is more distorted with increasing ionic radius of M^{3+}. The magnetic susceptibility and specific heat measurements show two kinds of anomalies, i.e., a broad maximum at 135–370 K (or a plateau at 22 K for La compound) and an anomaly at 4.5–12.5 K. It is considered that the magnetic behavior is due to the nature of the $Ru_2^{4.5+}O_9$ dimers, i.e., the antiferromagnetic coupling

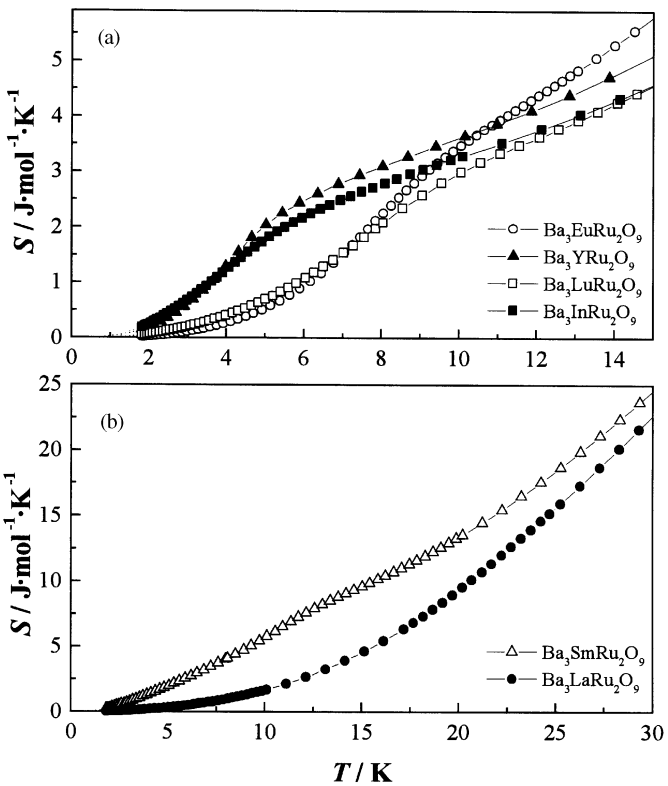

FIG. 8. Temperature dependence of the total entropy of $Ba_3MRu_2O_9$: (a) M = Y, In, Eu, and Lu, (b) M = La and Sm.

between two Ru ions in a $Ru_2^{4.5+}O_9$ dimer and the antiferromagnetic interaction between the $Ru_2^{4.5+}O_9$ dimers.

ACKNOWLEDGMENTS

One of the authors (Y. D.) thanks the Research Fellowships of the Japan Society for the Promotion of Science for Young Scientists. This work was supported by the Iwatani Naoji Foundation's Research Grant.

REFERENCES

1. Y. Maeno, H. Hashimoto, K. Yoshida, S. Nishizaki, T. Fujita, J. G. Bednorz, and F. Lichtenberg, *Nature* **372,** 532–534 (1994).
2. Y. Maeno, *Physica C* **282–287,** 206–209 (1997).
3. A. Callaghan, C. W. Moeller, and R. Ward, *Inorg. Chem.* **5,** 1572–1576 (1966).
4. Y. Doi and Y. Hinatsu, *J. Phys.: Condens. Matter* **11,** 4813–4820 (1999).
5. Y. Doi, Y. Hinatsu, K. Oikawa, Y. Shimojo, and Y. Morii, *J. Mater. Chem.* **10,** 797–800 (2000).
6. Y. Doi, Y. Hinatsu, K. Oikawa, Y. Shimojo, and Y. Morii, *J. Mater. Chem.* **10,** 1731–1737 (2000).
7. Y. Izumiyama, Y. Doi, M. Wakeshima, Y. Hinatsu, K. Oikawa, Y. Shimojo, and Y. Morii, *J. Mater. Chem.* **10,** 2364–2367 (2000).
8. Y. Izumiyama, Y. Doi, M. Wakeshima, Y. Hinatsu, Y. Shimojo, and Y. Morii, *J. Phys.: Condens. Matter* **13,** 1303–1313 (2001).
9. R. D. Burbank and H. T. Evans, *Acta Crystallogr.* **1,** 330–336 (1948).
10. J. Darriet, M. Drillon, G. Villeneuve, and P. Hagenmuller, *J. Solid State Chem.* **19,** 213–220 (1976).
11. M. Rath and Hk. Müller-Buschbaum, *J. Alloys Compd.* **210,** 119–123 (1994).
12. Von U. Treiber, S. Kemmler-Sack, A. Ehmann, H.-U. Schaller, E. Dürrschmidt, I. Thumm, and H. Bader, *Z. Anorg. Allg. Chem.* **481,** 143–152 (1981).
13. F. Izumi and T. Ikeda, *Mater. Sci. Forum* **321–324,** 198–203 (2000).
14. Y. Doi, Y. Hinatsu, Y. Shimojo, and Y. Ishii, *J. Solid State Chem.* **161,** 113–120 (2001).
15. Y. Doi and Y. Hinatsu, *J. Mater. Chem.*, in press.
16. J. T. Rijssenbeek, Q. Huang, R. W. Erwin, H. W. Zandbergen, and R. J. Cava, *J. Solid State Chem.* **146,** 65–72 (1999).
17. Hk. Müller-Buschbaum and B. Mertens, *Z. Naturforsch.* **51b,** 79–84 (1996).
18. Y. Doi, M. Wakeshima, Y. Hinatsu, A. Tobo, K. Ohoyama, and Y. Yamaguchi, *J. Mater. Chem.* 3135–3140 (2001).
19. P. Lightfoot and P. D. Battle, *J. Solid State Chem.* **89,** 174–183 (1990).
20. N. F. Mott and E. A. Davis, "Electronic Process in Non-Crystalline Materials," 2nd ed. Clarendon Press, Oxford, 1979.
21. J. T. Rijssenbeek, P. Matl, B. Batlogg, N. P. Ong, and R. J. Cava, *Phys. Rev. B* **58**(16), 10 315–10 318 (1998).